Int. J. Electrochem. Sci., 15 **(2020)** 879 – 888, doi: 10.20964/2020.01.56

International Journal of
ELECTROCHEMICAL
SCIENCE
www.electrochemsci.org

Effect of Ethanolamine on Corrosion Behavior of WB36CN1 Steel in Simulated Secondary Circuit of Pressurized Water Reactor

Jian Song, Zhiming Gao[*]*, Chenxi Liu, Zhihong Liu, Wenbin Hu*

School of Material Science and Technology, Tianjin University, Tianjin, 30072, China
Engineering Research Center of Composite and Functional Materials, Ministry of Education, Tianjin, 30350, China
[*]E-mail: gaozhiming@tju.edu.cn

Received: 5 September 2019 / *Accepted:* 30 October 2019 / *Published:* 30 November 2019

Effect of ethanolamine (ETA) on corrosion behavior of WB36CN1 low alloy steel in simulated pressurized water reactor (PWR) secondary circuit conditions was studied by electrochemical methods, scanning electron microscopy (SEM), 3D microscopy, and X-ray Photoelectron Spectroscopy (XPS). The polarization curve indicated that ETA can inhibit the cathode and anode processes, and corrosion current density decreased with increasing ETA concentration. EIS results showed that the charge transfer resistance and the oxide film resistance increased with increasing ETA concentration. The XPS results indicated that the main compositions of oxide film on the WB36CN1 steel were both Fe_3O_4 in the different solution (no ETA and 24ppm). SEM analysis suggested that the film oxide became more dense with increasing ETA concentration. Thus, the corrosion rate of WB36CN1 low alloy steel in the secondary circuit of PWR decreased with an increase of ETA concentration.

Keywords: WB36CN1 steel, PWR secondary circuit, ETA, SEM, XPS

1. INTRODUCTION

The corrosion of the secondary circuit pipeline of the pressurized water reactor affects the stable operation of the nuclear power plants, as the high temperature fluid can result in continuous thinning of the pipe wall. This type of corrosion is termed as flow accelerated corrosion (FAC), which is also occasionally referred to erosion-corrosion (E-C) in specific environments[1-2]. If undetected in time, the pipeline will suddenly rupture and release high temperature steam and water, which can injure plant personnel and damage nearby equipment. FAC is a predominant mode of failure of the pipelines in the secondary circuit. For example, feed water piping of the secondary side of Mihama-3 pressurized water reactor plant suddenly ruptured due to FAC in 2004[3-6]. FAC has slowly caught the researchers'

attention and efforts have been made to study the FAC in the secondary circuit including form, mechanism, specific cases and precautions.

In the high temperature fluid of PWR secondary circuit, metal pipeline made of carbon or low-alloy steel produces an oxide layer at the surface. The oxide layer exhibits typical black magnetite structure. High temperature fluid can make the protective oxide layer loose and accelerate the dissolution of the oxide layer on carbon or low-alloy steel, whereby the corrosion rate of pipeline steel increases[7]. Previous studies[8-11] have indicated that the process is related to electrochemical dissolution, mass transfer, fluid shear stresses and droplet wear. Furthermore, some studies have concluded that the major parameters, affecting the rate of FAC, include material factors, flow dynamics factors and environmental factors[12].

A few research studies about FAC of carbon steel or alloy steel have been reported. Jäppinen et al[13] concluded that some amines can reduce the corrosion rate of carbon steel in secondary side water. Zhang[14] reported that the maximum corrosion rate appears at the innermost side while the minimum corrosion rate at the outermost side of the elbow. In another study, Wang[15] stated that the impact angle plays a key role in the erosion-corrosion behavior of Q235 steel. However, there is still insufficient knowledge about the effect mechanism of ETA on FAC, especially from electrochemical aspect. In this study, the objective was to study the corrosion behavior of WB36CN1 low alloy steel in the PWR secondary circuit environment with different concentrations of ETA so as to determine the effect mechanism of ETA on the corrosion behavior of WB36CN1 steel.

2. EXPERIMENTAL

2.1. Material and solution

Table 1. Chemical constituent of WB36CN1 steel (wt-%)

C	Si	Mn	P	S	Cr	Ni	Cu	Mo	Nb	Al	Fe
0.152	0.376	0.866	0.0033	<0.008	0.20	1.13	0.636	0.267	0.0192	0.0097	balance

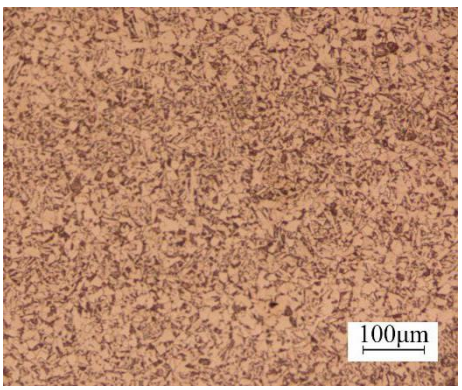

Figure 1. Microstructure of WB36CN1 low alloy steel

The chemical composition (wt%) of WB36CN1 low alloy steel was shown in Table.1. The microstructure of WB36CN1 steel after polishing and etched with 4% nitric acid was shown in Fig.1, which is composed of ferrite and bainite.

The WB36CN1 steel was machined into samples shown in Fig.2, and the thickness of sample was 2 mm. The samples were polished with SiC paper from 150 to 2000 grit. Then the samples were rinsed with deionized water and ultrasonically degreased with ethanol for 15 min, then blowdried in air and put in a drying dish for the following experiment.

The test solution was prepared from analytical reagent ETA, deionized water and sodium chloride to simulate PWR secondary cooling water. The NaCl (as impurity) concentration was 100 μg/L. The ETA concentrations were 0, 3, 6, 12, and 24 mg/L (ppm for a brief description in the following context), respectively. The testing solution, which was poured into the autoclave shown in Fig. 2, was deoxygenated by continuously purging nitrogen gas (99.999%) for 1 hour. The all experiments were performed at 270℃. The pressure of test environment was the saturated vapor pressure of the solution, which was approximately 5.5 MPa. The test rotating speed was adjusted to 500 r/min for simulating high temperature fluids.

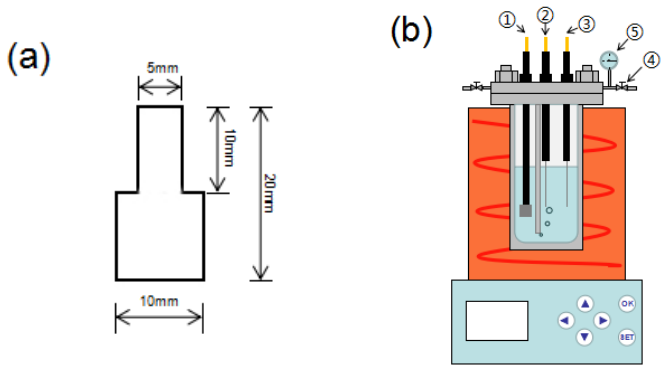

Figure 2. (a)Experimental sample and (b)schematic diagram of autoclave (①working electrode② reference electrode③counter electrode④gas valve⑤pressure gauge)

2.2 Electrochemical measurements

The electrochemical measurements were conducted by PARSTAT 2273 electrochemical test system. The working electrode was a WB36CN1 steel samples. Before the experiment, the samples were welded to wire, then wrapped in PTFE tape and inserted into the electrode holder. The reference electrode and counter electrode were both Pt wires. The autoclave was heated to 270℃ and held for half an hour before electrochemical testing. The potentiodynamic polarization curves were conducted from −0.6 V to 0.6 V (vs. OCP) at a scanning rate of 0.5 mV/s. The electrochemical impedance spectroscopy (EIS) measurements were performed at an alternating current signal amplitude of 20 mV and the test frequency ranged from 100 kHz to 10 mHz.

2.3 Surface morphology and Oxide film characterization

After being exposed in simulated PWR secondary cooling water for 6 h, the samples were rinsed with deionized water and dehydrated with ethanol. Then the samples were observed by scanning electron microscopic and 3D microscope VHX-2000, respectively.

2.4 Oxide film characterization

After samples immersed in PWR secondary cooling water for 6 h, the corrosion products were examined by using ESCALAB 250XI X-ray photoelectron spectrometer.

3. RESULTS AND DISCUSSION

3.1 EIS

The EIS measurements at various ETA concentrations in simulated PWR secondary cooling water are shown in Fig.3. It can be observed from the phase angle diagram that EIS exhibited two time constants. Thus, it indicated that two relaxation processes on the electrode surface, which may be due to the formation of an oxide film on the surface of the sample[16]. Therefore, EIS data was fitted by using the equivalent circuits shown in Fig.4 with ZsimpWin software, where R_s is solution resistance, Q_f corresponds to the capacitance of the corrosion film, R_f corresponds to the resistance of the corrosion film, Q_{dl} is the charge transfer capacitance of the electric double layer, and R_t, which indicates the speed of the electrochemical reaction on the sample surface and was often used to evaluate the corrosion resistance of the material, is the charge transfer resistance of the electric double, respectively[17]. The fitted results of the EIS parameters at all ETA concentrations are listed in Table 2.

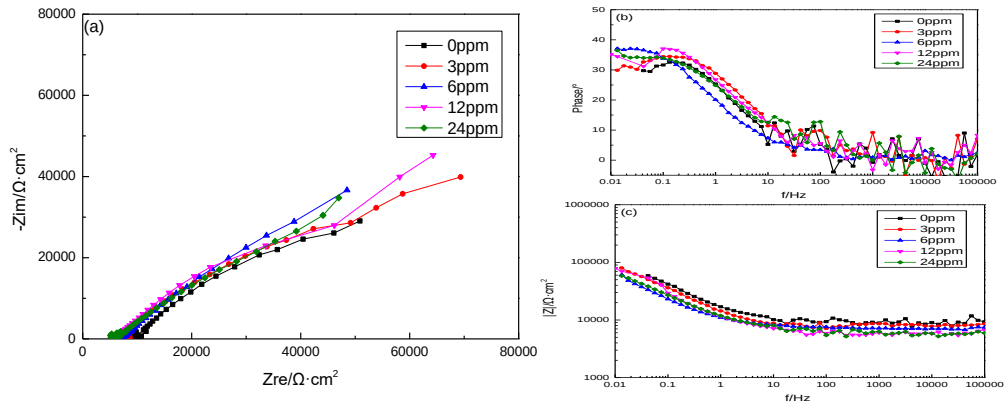

Figure 3. (a) Nyquist plot and (b), (c) Bode plot of WB36CN1 in solutions with different ETA concentrations.

As the concentration of ETA was increased, the solution resistance R_s gradually decreased due to the ability of ETA to increase the conductivity of the solution. Simultaneously, the charge transfer

resistance R_t became larger with increasing ETA concentration, which indicated that ETA can make the Fe atomic ionization and passing of charges through the electric double layer more difficult. Moreover, an increasing trend for the resistance of the corrosion film was observed. It indicated that the defects in the corrosion film on the sample surface became less with increasing ETA concentration, which makes the diffusion of carriers and external media in the oxide film more difficult, where the corrosion rate of samples became slower[18].

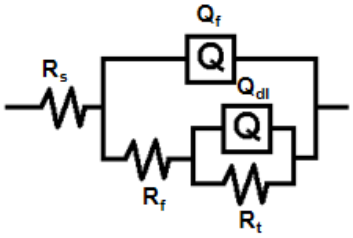

Figure 4. Electrochemical equivalent circuits for EIS fitting.

Table 2. Electrochemical parameters fitted from the measured EIS data.

	R_s ($\Omega \cdot cm^2$)	Y_f ($\Omega^{-1} \cdot cm^{-2} \cdot s^{-n}$)	n_1	R_f ($\Omega \cdot cm^2$)	Y_{dl} ($\Omega^{-1} \cdot cm^{-2} \cdot s^{-n}$)	n_2	R_t ($\Omega \cdot cm^2$)
0 ppm	9097	2.935×10^{-5}	0.611	6.069×10^{4}	5.767×10^{-6}	1	5.010×10^{4}
3 ppm	7910	3.370×10^{-5}	0.667	8.313×10^{4}	2.115×10^{-4}	1	5.235×10^{4}
6 ppm	7255	6.043×10^{-5}	0.641	6.331×10^{4}	1.141×10^{-4}	1	6.687×10^{4}
12 ppm	6028	3.940×10^{-5}	0.664	1.030×10^{5}	3.407×10^{-4}	1	1.701×10^{5}
24 ppm	5795	5.103×10^{-5}	0.526	1.753×10^{5}	2.016×10^{-4}	1	3.685×10^{5}

3.2 Polarization curve

The potentiodynamic polarization curves of WB36CN1 in simulated PWR secondary cooling water for different ETA concentrations are shown in Fig.5(a). According to the EIS results, the solution resistance was relatively large, thus, making it necessary to eliminate it. The equation was used:

$$|\Delta E| = |\Delta E_m| - |I| R_{sol} \qquad 3-1$$

where $|\Delta E|$ represents the absolute value of the true polarization value and $|\Delta E_m|$ represents the absolute value of the apparent polarization value including $|I| R_{sol}$. The result of polarization curves after eliminating the solution resistance is shown in Fig.5(b). The polarization curve parameters after eliminating the solution resistance are also listed in Table 3. It can be observed that all anodic process curves showed passivation behavior, which proved the formation of a dense passive film under the action of the anode current[19]. The passive current density decreased with increasing ETA concentration from 0 ppm to 24 ppm. In the meantime, as the ETA concentration increased, the cathodic current density gradually decreased. It indicated that ETA could inhibit both the anodic and cathodic reactions[20]. As shown in Table 3, the corrosion current density decreased and Tafel slope became larger with increasing ETA concentration. It showed that ETA inhibited the corrosion of WB36CN1 obviously as the concentration of ETA became larger.

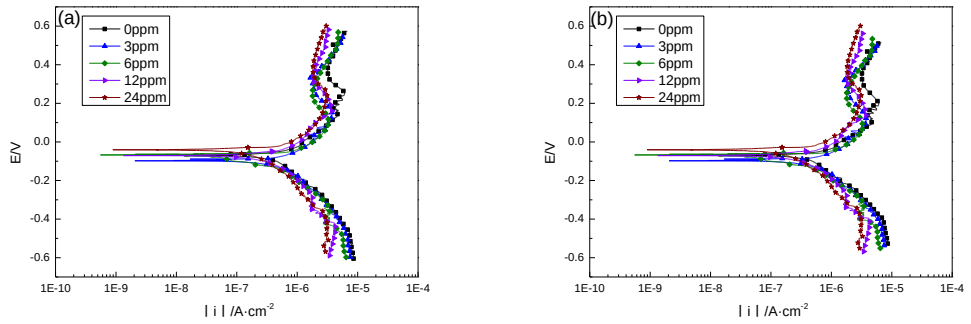

Figure 5. Polarization curves of WB36CN1 in simulated PWR secondary cooling water for different ETA concentrations ((a)original polarization curves, (b)polarization curves after eliminating the solution resistance)

Table 3. The related parameters of polarization curve at different ETA concentrations

ETA	i_{corr} (A·cm^{-2})	b_c (V/dec)
0 ppm	4.099×10^{-7}	-0.267
3 ppm	3.814×10^{-7}	-0.216
6 ppm	3.744×10^{-7}	-0.284
12 ppm	3.237×10^{-7}	-0.303
24 ppm	3.082×10^{-7}	-0.406

3.3 Characterization of macroscopic corrosion morphology

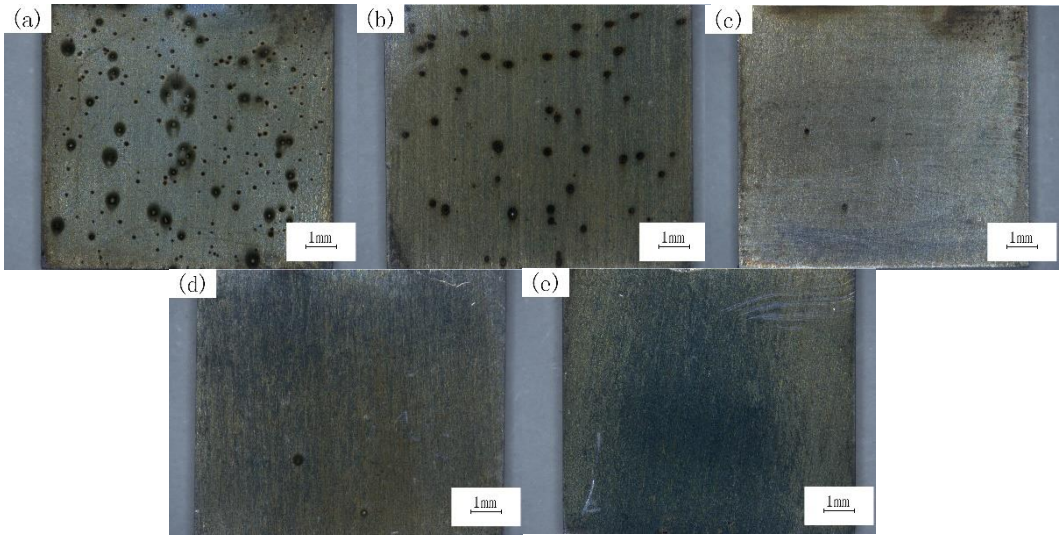

Figure 6. Macroscopic morphology of WB36CN1 steel after soaking for 6 h. ((a)0 ppm,(b)3 ppm,(c)6 ppm,(d)12 ppm,(e)24 ppm)

Fig. 6 shows the macroscopic corrosion morphology of WB36CN1 steel after soaking for 6 h in different concentrations of ETA, studied by 3D microscopy. As shown in Fig. 6, the extent of corrosion was observed to reduce with the concentration of ETA increasing from 0 ppm to 24 ppm. In the absence

of ETA in the solution, dense pitting occurred on the surface of the sample. As the concentration of ETA reached 6 ppm, the extent of pitting reduced significantly, and no pitting occurred on the sample surface for ETA concentration of 24 ppm. Simultaneously, the color of the surface oxidation product became dark with increasing ETA concentration. It indicated that ETA inhibited the corrosion process of WB36CN1 steel and prevented the contact of aggressive ions (Cl^-) with steel.

3.4 XPS

The XPS spectra of WB36CN1 steel in simulated PWR secondary cooling water with ETA concentrations of 0 ppm and 24 ppm are shown in Fig.7. The C1s, O1s, Fe2p and Fe3p peaks could be distinguished in the spectra.

It has been demonstrated in the previous studies that the peak positions of $Fe2p_{1/2}$ and $Fe2p_{3/2}$ depended on the ionic state of Fe, and the satellite peak positions of the $Fe2p_{1/2}$ and $Fe2p_{3/2}$ peaks were also sensitive to the oxidation state[21-25]. Thus, these peaks have been used to qualitatively determine the ionic state of iron, in the current study. The XPS spectra of Fe2p were fitted by using XPSPEAK software, as shown in Fig.8. $Fe2p_{3/2}$ did not exhibit any satellite peaks, and the peak positions of $Fe2p_{3/2}$ were 709.9eV and 709.7eV, whereas the peak positions of $Fe2p_{1/2}$ were 723.1eV and 723.1eV. The finding was consistent with the XPS spectrum of Fe_3O_4, thus, it could be concluded that the main component of the corrosion products in both environments was Fe_3O_4[26].

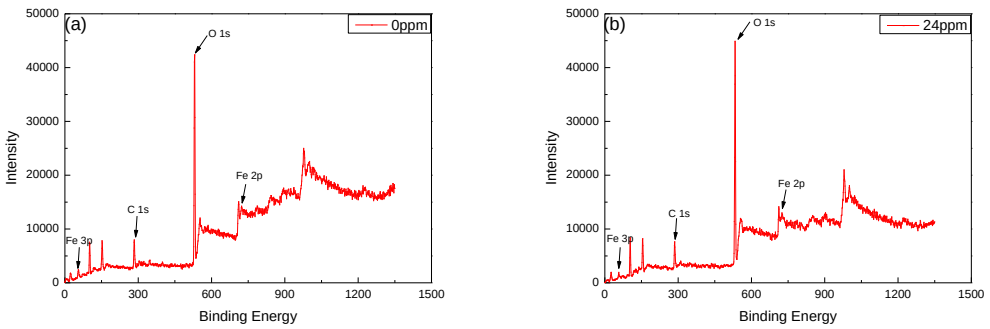

Figure 7. The XPS spectrum of WB36CN1 in different environments ((a)0 ppm ETA,(b)24 ppm ETA)

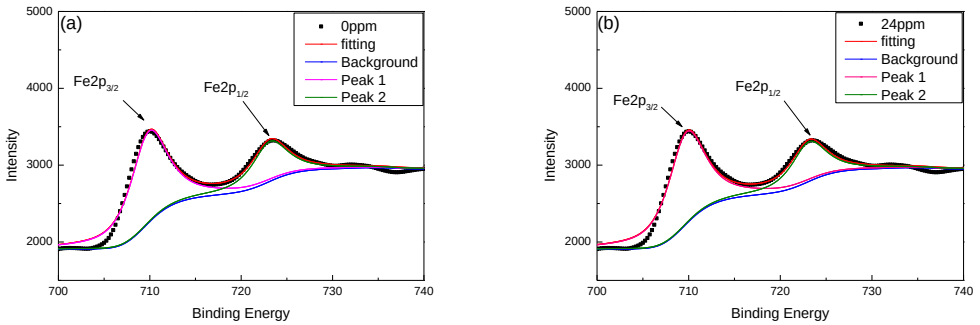

Figure 8. The Fe2p spectrum of WB36CN1 in different environments ((a)0 ppm ETA,(b)24 ppm ETA)

3.5 Characterization of microscopic corrosion morphology

Fig. 9 shows the SEM image of the surface morphology after soaking for 6 h in different concentrations of ETA. Corrosion product morphology of WB36CN1 steel was observed to be significantly affected by ETA concentrations. Flaky oxides were observed for all five cases, and the surface oxides became denser with increasing ETA concentration. In the absence of ETA in the solution, the surface oxide was observed to be the loosest, and the matrix of WB36CN1 steel was in more contact with the solution, which made the corrosion rate faster. In contrast, the surface oxides in the solution containing 24 ppm ETA were the densest, the metal matrix was not exposed, and the dense oxide hindered the progress of the corrosion reaction.

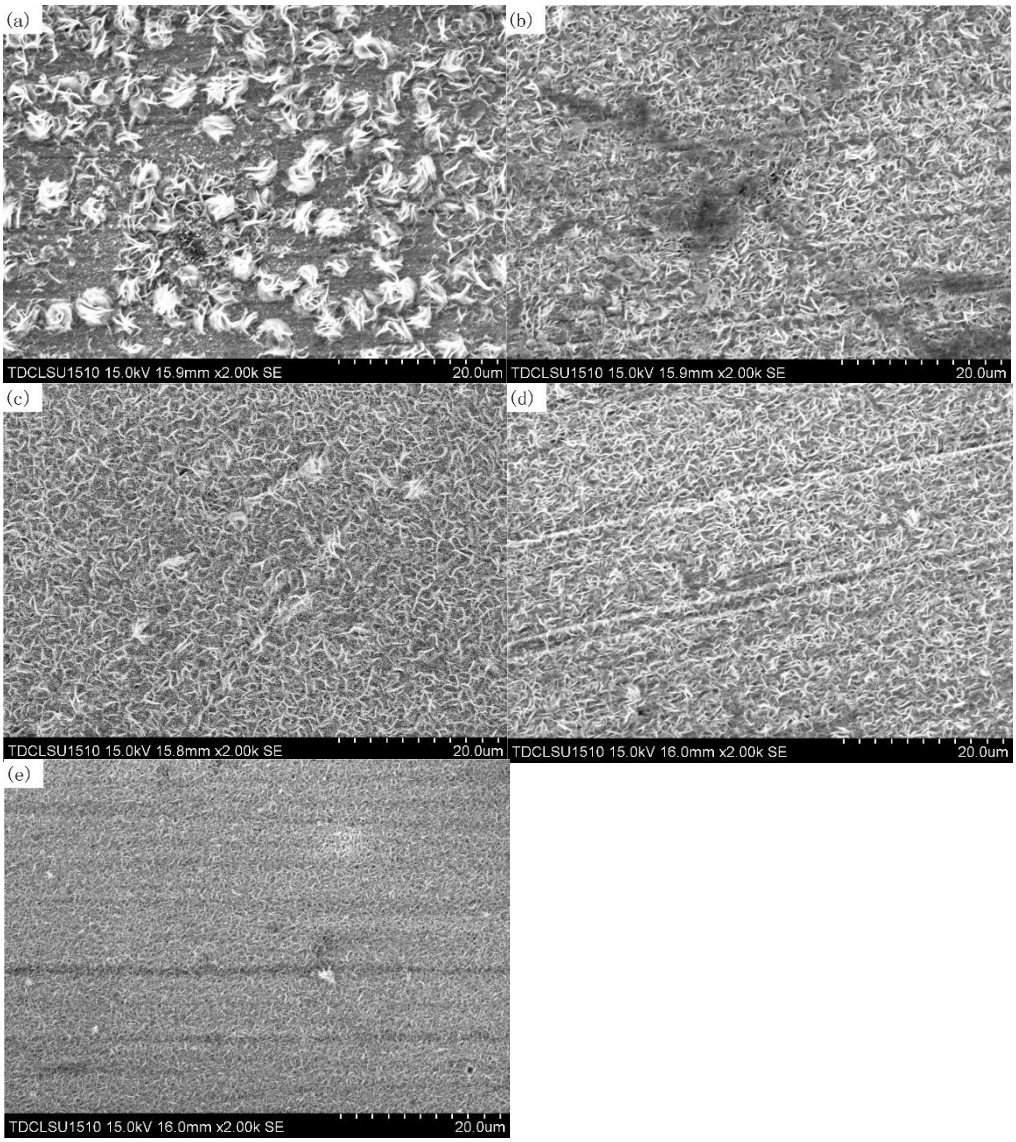

Figure 9. SEM of WB36CN1 steel after soaking for 6 h. ((a)0 ppm,(b)3 ppm,(c)6 ppm,(d)12 ppm,(e)24 ppm)

WB36CN1 steel reacted with oxygen-free water in a high temperature environment to form magnetite (Fe_3O_4). The reaction consisted of several steps, where iron atom was oxidized to form ferrous

hydroxide at first, and magnetite was subsequently formed by Schikorr reaction. The reactions are as follows:

$$Fe + 2H_2O \Rightarrow Fe(OH)_2 + H_2 \qquad 3-2$$

$$Fe(OH)_2 \Leftrightarrow Fe^{2+} + 2OH^- \qquad 3-3$$

$$Fe(OH)_2 \Rightarrow Fe_3O_4 + H_2 + 2H_2O \qquad 3-4$$

A combined form of the reaction can also be written, as shown in Eq.3-5. Simultaneously, magnetite layer underwent a Sweeton-Baes reaction at the oxide/solution interface to form a highly soluble product $Fe(OH)_b^{(2-b)+}$[27], as shown in Eq.3-6.

$$3Fe + 4H_2O \Rightarrow Fe_3O_4 + 4H_2 \qquad 3-5$$

$$\frac{1}{3}Fe_3O_4 + (2-b)H^+ + \frac{1}{3}H_2 \Leftrightarrow Fe(OH)_b^{(2-b)+} + \left(\frac{4}{3}-b\right)H_2O \qquad 3-6$$

With increasing ETA concentration, the pH of the solution and concentration of OH^- became larger. This is expected to facilitate the formation of $Fe(OH)_2$, which promotes the formation of more magnetite on the surface of WB36CN1 steel. Simultaneously, OH^- can inhibited the production of $Fe(OH)_b^{(2-b)+}$, which avoided the rapid dissolution of the magnetite. High pH also can change the structure of the surface oxide layer, thus, making it more denser, where the corrosion resistance of WB36CN1steel will be improved[28-29].

4. CONCLUSIONS

The effect of ETA concentration on the corrosion behavior of WB36CN1 steel were investigated by potentiodynamic polarization curves, EIS, XPS, 3D microscopy and SEM. The conclusions obtained are listed as follows:

(1) Addition of ETA can decreased the corrosion rate of WB36CN1 steel and inhibited the anodic and cathodic process.

(2) As the concentration of ETA increased, the extent of pitting on WB36CN1 steel decreased. When the ETA concentration was 6 ppm, pitting was fairly rare.

(3) The corrosion products of WB36CN1 steel were Fe_3O_4 in the environment with 0 ppm or 24 ppm ETA. As the ETA concentration increased from 0 ppm to 24 ppm, the pH of the solution increased, thus, also increasing the density of the oxide film on the steel surface.

ACKNOWLEDGEMENTS
The project was supported by National Natural Science Foundation of China (No.51871164, No. 51671144), Tianjin Science and Technology Project (No.18YFZCGX00050), and Shandong Taishan Industry Leading Talents Project(No.SF1503302301).

References

1. S. Uchida, M. Naitoh, H. Okada, Y. Uehara, S. Koshizuka, *Nucl. Eng. Des.*, 241 (2011) 4585.
2. M. H. Koike, *J. Nucl. Mater.*, 342 (2005) 125.

3. X. L. Zhu, X. F. Lu, X. Ling , *Mater. Corros.*, 64 (2013) 486.
4. M. El-Gammal, H. Mazhar, J. S. Cotton, C. Shefski, J. Pietralik, C. Y. Ching, *Nucl. Eng. Des.*, 240 (2010) 1589.
5. OKADA. Hidetoshi, UCHIDA. Shunsuke, *J. Nucl. Sci. Technol.*, *48* (2011) 65.
6. M. Naitoh, S. Uchida, S. Koshizuka, H. Ninokata, A. Minato, H. Saitoh, *Heat Transfer Eng.*, *29* (2008) 712.
7. R. B. Dooley, V. K. Chexal, *Int. J. Pressure Vessels Piping*, *77* (2000) 85.
8. W. H. Ahmed, *Ann. Nucl. Energy*, *37* (2010) 598.
9. G. A. Zhang, Y. F. Cheng, *Corros. Sci.*,*52* (2010) 2716.
10. V. Kain, *Procedia Eng.*, 86 (2014) 576.
11. J. A. Wharton, R. J. K. Wood, *Wear*, 256 (2004) 525.
12. S. Uchida, M. Naitoh, Y. Uehara, *J. Nucl. Sci. Technol.*, *45* (2008) 1275.
13. E. Jäppinen, T. Ikäläinen, S. Järvimäki, T. Saario, K. Sipilä, M. Bojinov, *J. Mater. Eng. Perform.*, *26* (2017) 1.
14. G. A. Zhang, L. Zeng, H. L. Huang, X. P. Guo, *Corros. Sci.*, 77 (2013) 334.
15. Q. Y. Wang, S. L. Bai, .Z. D. Liu, *Tribol. Lett.*, 53 (2014) 271
16. S. Zhang, *Int. J. Electrochem. Sci.*, 12 (2017) 2453.
17. B. Yang, M. C. Li, M. Y. Yao, *Acta Metall. Sin.*, 46 (2010) 946-950.
18. L. Q. Wang, Z. M. Gao, Y. J. Liu, *Int. J. Electrochem. Sci.*, 14 (2019) 161.
19. S. Zhang, *Int. J. Electrochem. Sci.*, 13 (2018) 3246.
20. J. Z. Wang, J. Wang, *J. Mater. Sci. Technol.*, 31 (2015) S1005030215000791.
21. A. P. Grosvenor, B. A. Kobe, M. C. Biesinger, *Surf. Interface Anal.*, 36(2004) 1564.
22. A. Mekki, D. Holland, C. F. Mcconville, *J. Non-Cryst. Solids*, 208 (1996) 267.
23. T. Yamashita, P. Hayes, *J. Electron Spectrosc. Relat. Phenom.*, 152 (2006) 6.
24. S. J. Roosendaal, B. V. Asselen, J. W. Elsenaar, *Surf. Sci.*, 442 (1999) 329.
25. P. C. J. Graat, M. A. J. Somers, *Appl. Surf. Sci.*, 100 (1996) 36.
26. T. Yamashita, P. Hayes, *Appl. Surf. Sci.*, 254 (2008) 2441.
27. F. H. Sweeton, *J. Chem. Thermodyn.*, 2 (1970) 479.
28. J. B. Huang, X. Q. Wu, E. H. Han, *Corros. Sci.*, 51 (2009) 2976.
29. H. Sun, X. Q. Wu, E. H. Han, *Corros. Sci.*, 59 (2012) 334.